Comparison of Electromagnetically Induced Transparency Performance in Metallic and All-Dielectric Metamaterials

Jie Hu, Tingting Lang, Zhi Hong, Changyu Shen, and Guohua Shi

***Abstract*—Analogs of Electromagnetically Induced Transparency (EIT) in metamaterial have undoubtedly become a research hotspot in recent years. In this paper, we summarized some of the literature on EIT published to date and compared their performance. Then, we designed two kinds of metamaterials using aluminum and silicon. Both have the similar glasses-shaped structure of a periodic lattice with one bar resonator and two split ring resonators. We analyzed and compared the EIT performance in the near infrared waveband of these two metamaterials. The metallic EIT metamaterials with large radiation loss and ohmic heat loss have a smaller Q-factor than the dielectric counterpart with less energy loss, while having a higher sensitivity toward the ambient refractive index. The Q-factor of our designed aluminum metamaterial and silicon metamaterial are 10.06 and 412.6, respectively. Their sensitivities are 1642.97 nm/RIU and 433.05 nm/RIU, respectively, which are higher than most of their counterparts in the same waveband in the other literature. For the application of slow light, the dielectric metamaterials with higher Q-factor are far superior to the metallic metamaterials in the same waveband and comparable propagation distance. The group index of the aluminum metamaterial is 42.9, and the group delay is 0.01 ps in the near infrared waveband. For the silicon metamaterial, the group index is approximately 1907.1, and the group delay is 0.89 ps within the transmission window in the near infrared waveband; these values are both higher than most counterparts in the same waveband in other literature. The EIT metamaterials that we designed have excellent performance, and to the best of our knowledge, this paper presents the first detailed comparison of EIT metamaterials made of dielectric and metal with similar structure; this paper may have certain instructive meaning for further research on metamaterial analogues of EIT in the future.**

Manuscript received December 22, 2017; revised February 5, 2018; accepted February 6, 2018. Date of publication February 9, 2018; date of current version March 2, 2018. This work was supported in part by the Public Projects of Zhejiang Province (LGG18F050003), in part by the National Major Scientific Research Instrument Development project of the Natural Science Foundation of China under Grant 61727816, in part by the National Natural Science Foundation of China under Grant 61377108 and Grant 61405182, in part by the National Instrumentation Program under Grant 2016YFF0102000, and in part by the Frontier Science research project of the Chinese Academy of Sciences under Grant QYZDB-SSW-JSC03. *(Corresponding author: Tingting Lang.)*

J. Hu, T. Lang, and C. Shen are with the Institute of Optoelectronic Technology, China Jiliang University, Hangzhou 310018, China (e-mail: 1225297792@qq.com; langtingting@cjlu.edu.cn; shenchangyu@cjlu.edu.cn).

Z. Hong is with the Centre for THz Research, China Jiliang University, Hangzhou 310018, China (e-mail: hongzhi@cjlu.edu.cn).

G. Shi is with the Key Medical Optics Laboratory of Jiangsu Province, Suzhou Institute of Biomedical Engineering and Technology, Chinese Academy of Sciences, Suzhou 215163, China (e-mail: ioe_eye@126.com).

Color versions of one or more of the figures in this paper are available online at http://ieeexplore.ieee.org.

Digital Object Identifier 10.1109/JLT.2018.2804336

***Index Terms*—Metamaterials, Q-factor, refractive index, slow light.**

I. Introduction

IF A substance can strongly absorb the light of a particular frequency, it is opaque for this probe light. However, if we add a pump laser with a frequency that can also be absorbed by this substance, then the absorption of the probe light can be greatly reduced so that the substance becomes transparent to the probe light. This fascinating phenomenon is called Electromagnetically Induced Transparency (EIT). Since Steven Harris and his research team presented an early theory of EIT in 1989 and observed this phenomenon for the first time in strontium vapor in 1990 [1], this phenomenon has drawn great attention. EIT can be explained by the destructive quantum interference between two different excitation transition pathways; this interference leads to a transparency window in the broad absorption band. The realization of EIT is usually accompanied by a strong dispersion phenomenon, which can also dramatically reduce the group velocity [2] and enhance nonlinear interactions [3].

However, EIT in the atomic system must be implemented in very stringent experimental conditions, such as high intensity optical pumping and cryogenic temperatures. Such demands seriously limit practical applications, especially when integration is involved. How to achieve the analogues of EIT in classical systems without these cumbersome experimental conditions has been widely studied.

C. L. Garrido Alzar's research group [4] designed a system consisting of two coupled harmonic oscillators and added a harmonic driving force to excite the system; this EIT-like phenomenon in a classical system was realized in 2002. They also described a simple experiment with two linearly coupled RLC circuits. Scientists gradually realized that the mechanism of EIT in atomic systems can be analogous to the classical theory, and EIT-like phenomenon can be imitated in classical systems.

For instance, EIT in waveguides with resonators [5]–[7] is excited by the destructive interference between different couplings, which were studied in the beginning. In these systems, the structure consists of a waveguide and two or more side-coupled resonators. The resonators often are ring or microsphere resonators in all-dielectric systems [8]–[10] or cavities in plasmonic systems [11]–[14]. If the waveguide is only side-coupled with one resonator, a dip in transmission spectrum is

observed. If one more side-coupled resonator is added, which could couple with the waveguide with lower loss, this second coupling suppresses the first coupling, and the destructive interference between these two "excitation paths" will generate a transmission peak in the broader absorption dip, which is so called EIT. In recent years, EIT based on metamaterials, which is described below, has become an important kind of implementation of EIT in classical optical systems.

In this paper, we sorted through some of the literature about EIT published so far. Then, we designed two metamaterials with similar structures but different materials (aluminum and silicon). Both are composed of a periodic lattice of a bar resonator and two split ring resonators (SRRs). We analysed and compared the EIT performances between the metallic and all dielectric metamaterials in the near infrared waveband. We also extended the comparison to applications in slow light and refractive index sensing fields.

II. Generalization of EIT in Metamaterials

Electromagnetic metamaterials are artificially engineered composites with subwavelength structures, whose physical properties such as permeability, dielectric constant, and conductivity can be arbitrarily designed by changing the structure of the periodic lattice and its size. Metamaterials can easily have properties that are not found in nature. Many novel applications have been realized by metamaterials, such as cloaking devices [15], superlens [16], perfect reflection or absorption filters [17], and non-diffracting beam sources [18]. Obtaining the analogues of electromagnetically induced transparency based on a metamaterial is also an interesting topic.

A. EIT in Metallic Metamaterials

Metal is initially used to achieve a metamaterial based EIT phenomenon. According to the formation mechanism of EIT, it can be realized by the coupling of two "bright modes" or the coupling of a "dark mode" and a "bright mode (or radiative mode)". The "bright mode" means the resonance that can be excited by the incident light directly, while the "dark mode" refers to the resonance that cannot be excited by incident light directly.

A. Fedotov's research group [19] designed a planar periodic array of asymmetrically split-rings consisting of two arcs with different lengths and discussed three resonant modes with two polarizations of the incident light. Then, the EIT-like phenomenon was observed by breaking the symmetry of SRR [20]. N. Papasimakis' research group [21] proposed a structure with a fish-scale metallic pattern etched on both sides of the PCB laminate. The incident electromagnetic wave aroused the reverse currents at the surface of the metal stripe on both sides of PCB laminate; the destructive interference of the radiation electromagnetic field excited by the counter-propagating currents caused a phenomenon analogous to EIT. The resonances excited in antiphase interfere with each other destructively in single [22] and double layer structures [23] were subsequently published.

The EIT based on interference between the guided mode resonance (GMR) in the SiN_x waveguide layer and the resonance in the upper structure of metamaterial [24], proposed by Zhi Hong's research group, is another kind of EIT realization mechanism. A similar EIT phenomenon in metallic or plasmon metamaterial based on guided mode resonance can also be found in reference [25].

Previously mentioned EIT is based on the mutual inhibition between two "bright modes". Another kind of EIT realization mechanism is when the "dark mode", excited by coupling with the "bright mode", suppresses the "bright mode" and generates a sharp transparent window. Various structures have been proposed, among which the coupling between split-ring resonators (SRRs) [26], coupling between bar resonators along different directions [27]–[29], or coupling between bar resonator and SRRs [30]–[36] are typical examples.

Shuang Zhang's research group [37] proposed a periodic structure consisting of silver strips with different directions and observing the EIT-like phenomenon in the near infrared waveband. A simple silver strip, which is parallel to the electric field polarization of normally incident light, is an excited optical dipole antenna and thus serves as the "bright atom". The "dark atom" is composed of two parallel silver strips that are perpendicular to the "bright atom" with a small separation. The "dark mode" couples with the "bright mode" and suppresses it, thus yielding the EIT phenomenon accompanied by a strong dispersion effect where the group index (n_g) can reach 41. One year later, Na Liu's research group [38] proposed a kind of bilayer structure with the same mechanism. The next year, they experimentally demonstrated a complementary planar metamaterial analogue of EIT at optical frequencies [39]. They immersed the metamaterial into different concentrations of glucose solutions and detected the drift of the EIT peak. The sensitivity towards the external refractive index is 588 nm/RIU.

Another common type of EIT is based on the destructive interference between the localized surface plasmon (LSP) resonance and the LC resonance. In 2012, Xiaojun Liu proposed an EIT metamaterial, whose unit cell consists of a cut wire and a pair of SRRs [40]. The incident electric field is oriented along the sole-wire and excites a typical LSP resonance directly. The fundamental LC resonance in the SRRs cannot be excited by the incident light directly but can be excited by coupling with the electromagnetic field generated by the "bright" resonator. Xueqian Zhang's research group [41] proposed a polarization-independent EIT in a fourfold symmetric terahertz metamaterial with four SRRs placed in the four quadrants formed by the cross of two aluminum bars. It is worth mentioning that active control of EIT in metamaterials with electric currents [42] or ultrafast optical pulses [43] have also recently been studied.

So far, the plasmonic EIT phenomena often arise from the electric-electric coupling. However, the magnetic interactions between bright and dark modes can also generate the plasmonic EIT effect. The magnetic interactions between bright and dark modes are intriguing because the magnetic response has lower radiation loss than the electric case. The PIT metamaterial, whose unit cell consists of three erected U-shape SRRs [44], was proposed in 2012 and can exhibits plasmonic EIT

phenomenon with magnetic dipolar interaction between magnetic metamolecules. The next year, Farbod Shafiei's research group [45] designed a metamolecule consisting of four closely spaced gold nanoparticles, and the first magnetic-based Fano scattering resonance at optical frequency was observed by introducing the small structural asymmetries in the assembled nanoring.

B. EIT in All-Dielectric Metamaterials

Most previous studies of metamaterial based EIT employ metallic resonators and related planar structures based on conduction current oscillation. The main limitation of these metallic systems is the huge non-radiative loss due to ohmic damping, which restricts the achievable quality-factor (Q-factor) to 10. The Q-factor is a parameter calculated by the following formula:

$$Q = \frac{f_0}{FWHM} \tag{1}$$

where the f_0 is the frequency of maximum transmission at the EIT window, and the *FWHM* is the full width at half maximum.The utilization of high-refractive-index dielectric particles is expected to solve the issue of material (non-radiative) loss, since the displacement current in dielectric metamaterials replaces the conduction current in metallic counterparts. These high-refractive-index dielectric particles exhibit electric dipoles, magnetic dipoles, and higher order Mie resonances [46], [47], with minimal absorption loss. Coupling between all-dielectric nanoresonators can lead to similar phenomena, but with significantly enhanced efficiency compared to their metallic counterparts. Thus, EIT based on all-dielectric metamaterials has attracted increasing number of scholars to research.

Fuli Zhang's research group referenced the mechanism in [26] and experimentally demonstrated a magnetically coupled EIT analogy phenomenon in a dielectric metamaterial within microwave band with a group index of 55 [48]. Jianfa Zhang's research group imitated the structure in [27], and numerically investigated the EIT-like behaviour in all dielectric metamaterials in the near infrared band [49]. The Q-factor of the simulated result can be 12000 and the group index reaches 207. Yuanmu Yang's research group experimentally demonstrated an analogue of EIT using silicon-based metasurfaces [50]. The structure is a periodic unit consisting of a rectangular bar resonator and a ring resonator. The Q-factor can reach tens of thousands in numerical simulation, and the experimental result is 483 due to the limitations in manufacturing process. For the sensitivity towards refractive index, it is 379 nm/RIU. There are also other structures with similar forming mechanisms proposed, such as a windmill type metamaterial consisting of two dumbbell dielectric resonators [51], and a periodic array consisting of a bar and six bricks made of titanium oxide [52]. E. Petronijevic's research group put a thin layer of $Ge_2Sb_2Te_5$ on top of the resonators to tune the optical response and realized all-optical tuning of EIT-like phenomenon [53].

Another approach for EIT realization is the utilization of guided mode resonance (GMR). Pei Ding's research group theoretically demonstrated an analogue of EIT in an all-dielectric metamaterial-waveguide system that consists of a two-dimensional silicon nanopillar array on top of a dielectric slab waveguide [54]. The overlap and interference between the GMR and magnetic resonance in the silicon nanopillar generate this EIT peak in visible frequencies. The Q-factor can reach 38 and the group index is 13.8. Sun-Goo Lee's research group presented an EIT system based on guided-mode resonances. The system is composed of two planar dielectric waveguides and a subwavelength grating [55]. The EIT is generated by coupling the two guided mode resonances with low- and high-quality factors.

C. Applications Based on EIT Metamaterial

The continuous steep change of the transmission phase within the transmission window leads to a strong dispersion so that the analogue of EIT is always accompanied by a slow-light effect [42], [43], [56]. To clearly understand the slow light effect of the proposed metamaterials, the time delay is defined as [57]

$$\tau_g = -\frac{d\varphi(\omega)}{d\omega} \tag{2}$$

where φ is the transmission phase shift in the metamaterial. The group index is calculated as

$$n_g = \frac{c}{v_g} = \frac{c}{D} \times \tau_g = -\frac{c}{D} \times \frac{d\varphi(\omega)}{d\omega} \tag{3}$$

where c is the velocity of light in free space, v_g and τ_g are group velocity and delay time in the metamaterial, and *D* is the thickness of the metamaterial. Another formula [35] for calculating slow light effects through the S-parameter retrieval method [58], [59] is recognized by many scholars, although this calculation method has little deviation because the S-parameter retrieval method is an equivalent approximation.

On the other hand, there are many instances where adjusting and controlling the optical response can be used to turn off or on the EIT phenomenon, as mentioned above. Hence the EIT metamaterial can also be designed to realize a photo switch [43], [53].

Out of the many existing applications, one of most interesting is optical sensing. The EIT-like spectrum is a transmission peak (or reflection peak in some of the metallic metamaterials) among the broad absorption dip. This peak often has a narrow linewidth, and the wavelength shift is easy to distinguish. Therefore, the wavelength or frequency shift of the EIT peak can be used for external refractive index detection. To the best of our knowledge, there is an interesting phenomenon where the metallic EIT metamaterial generally has higher refractive index sensitivity than its all-dielectric counterparts, although the former has smaller Q-factor than the latter. The sensitivity of the metallic structure can easily exceed the hundreds order in near infrared band [27], [28], [39], [60], [61]. However, the sensitivity of all-dielectric metamaterials is usually in the order of hundreds [50], [57], [62]. Furthermore, a majority of metallic designs in the above metamaterials lie flat on substrates, thus a rather appreciable fraction of the plasmon energy of metallic structure would distribute in the substrate below, which limits the sensitivity towards ambient medium. Some scholars alter the layout of the structure, such as by erecting the split ring [63],

[64], or by raising the metal structure [28], so that there would be more surface plasmon energy distributing in the surrounding environment, and thus can further increase the sensitivity of the metallic EIT metamaterial. Considering the metallic metamaterials and all-dielectric metamaterials have different strengths and weaknesses in terms of sensitivity and linewidth, so the figure of merit (FOM) parameter is often used as another important sensor of performance index and is determined as

$$\mathrm{FOM} = \frac{S}{FWHM} \tag{4}$$

where *S* is the sensitivity towards ambient refractive index, and the *FWHM* is the full width at half maximum of the EIT peak.

We summarized the above investigation of metallic and all-dielectric metamaterial based EIT phenomena in table 1. Their performance including the Q-factor, FOM, refractive index sensitivity, and group delay are also compared.

III. Design and Simulation

To make a better comparison, metamaterials with similar structure but different material (metal and dielectric) for EIT realization are designed and simulated. The chosen structure is a glasses-shaped unit cell structure composed of periodically arranged bar and ring resonators. Aluminum and silicon (n = 3.7) are chosen as the representative materials. The complex dielectric constant of aluminum is modeled by the Nth order model fitting (N = 7) to approach experimental data. One lattice unit consists of one bar resonator (glasses frame) and two split ring resonators (SRRs, lenses of glasses) on the bulk fused silica substrate (n = 1.48), as shown in Fig. 1(a) and (b), respectively. The protrusion at the middle of the bar is an isosceles trapezoid. Fig. 1(a) shows the aluminum metamaterial. The periods of the unit cells are equal in both x and y directions, where $P_{x1} = 650$ nm and $P_{y1} = 450$ nm. The external and inside internal radii of the SRR are $R_{\mathrm{out}1} = 110$ nm and $R_{in1} = 65$ nm, respectively. The gap of the split in SRR is $\mathrm{gap}_1 = 60$ nm. The length and width of the bar resonator is $L_1 = 570$ nm, $w_1 = 50$ nm. The size of the isosceles trapezoid is $a_1 = 160$ nm, $\mathrm{b}_1 = 60$ nm, $\mathrm{h}_1 = 50$ nm. The spacing of the SRR and the bar resonator is $S_1 = 40$ nm. The gap between the two centres of the SRRs is $dx_1 = 340$ nm. The thickness of the aluminum structure is $t_1 = 70$ nm. The geometrical parameters of the silicon structure in Fig. 1(b) are $P_{x2} = 1540$ nm, $P_{y2} = 1000$ nm, $L_2 = 1000$ nm, $w_2 = 215$ nm, $a_2 = 380$ nm, $\mathrm{b}_2 = 120$ nm, $\mathrm{h}_2 = 130$ nm, $R_{\mathrm{out}2} = 315$ nm, $R_{in2} = 195$ nm, $\mathrm{gap}_2 = 70$ nm, $S_2 = 75$ nm, $dx_2 = 780$ nm, and $t_2 = 140$ nm. The difference in the geometrical parameters is caused by the difference of material parameters. These results in their EIT spectra are approximately in the same waveband. Three-dimensional full wave electromagnetic field simulations are performed by the finite integral method. Perfectly matched layers are used in the wave propagating direction of the *z*-axis, while periodic boundary conditions are utilized in both the *x* and *y* directions. We assume the incident light, with a wave vector of *k,* to be a plane wave that propagates along the *z*-axis. The electric and magnetic fields of the incident light are polarized along the *x* and *y*-axes, respectively, as shown in Fig. 1(a) and (b).

IV. Results and Discussion

A. EIT Performance

The finite integral method is used to calculate the transmission spectra of the designed metamaterials. The incident electric field E is oriented along the *x*-axis, and a transmission peak approximately 1530 nm is observed for the aluminum metamaterial, as shown in Fig. 2(a). This is the analogue of EIT caused by the destructive interference between the "bright modes" generated by the bar resonator and the "dark mode" generated by the pair of SRRs. The Q-factor of this metallic metamaterial is approximately 10. The absorption spectrum, calculated by

$$A = 1 - T - R \tag{5}$$

is also shown in Fig. 2(a), which indicates the large loss limiting its transmission intensity and Q-factor.

To further investigate the origin of the EIT peak, more simulations are performed. The transmission spectrum of the sole-wire array is shown in Fig. 2(b) with the black curve; there is a transmission dip at approximately 1550 nm because of the typical LSP resonance. However, in this case, the LC resonance in the sole SRR pair (red curve) cannot be excited directly due to the structural symmetry with respect to the exciting field. With E along the *y*-axis, on the other hand, a narrower LC resonance is easily excited in the sole SRR pair and the transmission spectrum (blue curve) shows a dip at nearly the same wavelength. Furthermore, if the energy loss in a system is larger, the amplitude transmission in the spectrum at the resonance dip would be lower; the resonance dip then looks wider, and the Q-factor will be lower. For example, the LSP resonance in the bar resonator ("radiative mode" or "bright mode") has larger radiation loss than the LC resonance in the SRRs ("dark mode"), the resonance dip of the "radiative mode" (black curve) is wider than the "dark mode" (blue curve), and the Q-factor of the "radiative mode" is lower than the "dark mode". When these two types of resonators are arranged in close proximity to each other within a unit cell, the LSP resonance induces a magnetic field around the bar, which traverses the SRRs and excites the surface current and an electric field along open end direction (the *y* axis); a typical EIT such as spectral response is then observed, as shown in Fig. 2(a).

Fig. 2(c) shows the transmission and absorption spectrum of the silicon metamaterial with an incident plane wave having the electric field E polarized along the *x*-axis; there is also a transmission peak at approximately 1540 nm with little absorption loss, which is caused by the destructive interference between the "dark mode" and the "bright mode". The *FWHM* of this silicon metamaterial is much smaller than its aluminum counterpart and the Q-factor is approximately 412.6. The transmission spectra of the sole silicon wire and sole silicon SRR pair pattern are shown in Fig. 2(d). If the incident E-field is oriented along the *x*-axis, the electric dipole excited in the silicon bar replaces the LSP resonance in the metallic bar and then serves as an electric dipole antenna which couples strongly to free-space excitation and forms the "bright mode" resonance. We can see that there is a broad transmission dip at approximately 1510 nm with the black curve in Fig. 2(d). However, no

TABLE I
THE PERFORMANCE COMPARISON OF VARIOUS METALLIC AND ALL-DIELECTRIC METAMATERIAL BASED EIT STRUCTURES WITH Q-FACTOR, REFRACTIVE INDEX (RI) SENSITIVITY, FIGURE OF MERIT (FOM) AND GROUP DELAY DISPLAYED

Structure	Wavelength band	Q-factor	RI sensitivity (S)	FOM (S/*FWHM*)	Group delay	Reference and year
Silver bar resonators with different directions	Near infrared waveband	~650 (with gain medium) ~78 (without gain medium) **(Simulation)**	680 nm/RIU **(Simulation)**	400 (with gain medium) ~25 (without gain medium) **(Simulation)**		[27] 2011
The bar-shaped grooves with different length in the gold film	Near infrared waveband	~35 **(Simulation)**	928.9 nm/RIU **(Simulation)**	19.2 **(Simulation)**		[28] 2013
Combination of copper bar resonator and SRR (like steering wheel)	Microwave waveband		9.2 mm/RIU **(Experiment)**	11.9 **(Experiment)**		[34] 2016
The bar-shaped grooves with different direction in the gold film	Near infrared waveband	~10 **(Experiment)**	588 nm/RIU **(Experiment)**	3.8 **(Experiment)**		[39] 2010
Silicon bar resonator + Silicon ring resonator	Near infrared waveband	30000 **(Simulation)** 483 **(Experiment)**	379 nm/RIU **(Experiment)**	103 **(Experiment)**		[50] 2014
Silicon nanobars (like a cross)	Near infrared waveband	2400 **(Simulation)**	294 nm/RIU **(Simulation)**	42 **(Simulation)**	0.65 ps	[57] 2017

Structure	Wavelength band	Q-factor	Group index	Group delay	Reference and year
Metal ring + Silicon nitride waveguide layer	Mid - infrared waveband	7000 **(Simulation)**	770		[24] 2017
Silver bar resonators with different direction	Near infrared waveband	411 **(Simulation)**	300		[29] 2016
Copper bar resonator and copper split square ring resonator	Microwave waveband	35 **(Simulation)**	140		[32] 2014
Silver bar resonators with different direction	Visible light and near infrared waveband		41		[37] 2008
Aluminum bar resonator + Aluminum split square ring resonator	Terahertz waveband	~6 **(Simulation)**		~3 ps	[42] 2016
Aluminum bar resonator + Aluminum split square ring resonator (integrated with photoconductive silicon)	Terahertz waveband	~7 **(Simulation)**		5.74 ps	[43] 2012
Three upstanding split square ring resonator with six-fold rotational symmetry	Microwave waveband	130.3 **(Simulation)**	427	1.19 ns	[35] 2016
Ceramic bricks	Microwave waveband	~40 **(Experiment)**	55		[48] 2014
silicon nanobars with different direction	Near infrared waveband	12000 **(Simulation)**	207		[49] 2014
Titanium oxide (TiO2) windmill Configuration	Terahertz waveband	~14 **(Simulation)**	100		[51] 2013
Silicon nanopillars + polystyrene waveguide layer	Visible light waveband	38 **(Simulation)**	13.8		[54] 2015
Ceramic wires with different length	Microwave waveband	62 **(Experiment)**		1.97 ns	[56] 2014

Structure	Wavelength band	Q-factor	RI sensitivity	FOM	Group index	Group delay	Reference and year
Glasses-Shaped structure	Near infrared waveband	10.06 (Aluminum) 412.6 (Silicon)	1642.97 nm/RIU (Aluminum) 433.05 nm/RIU (Silicon)	11.0 (Aluminum) 116.7 (Silicon)	42.9 (Aluminum) 1907.1 (Silicon)	0.01 ps (Aluminum) 0.89 ps (Silicon)	This paper

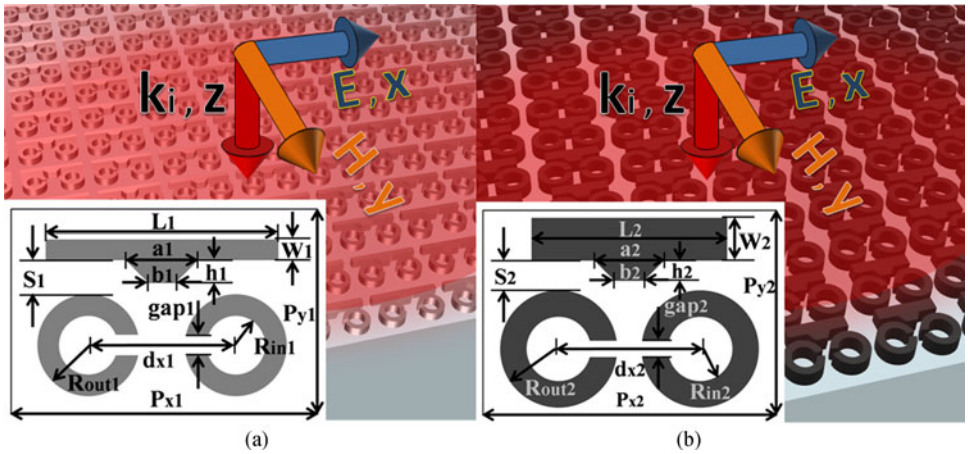

Fig. 1. Schematic diagram of the designed (a) aluminum metamaterial and (b) silicon metamaterial for comparing the EIT performance. The polarization direction of the incident light is also presented.

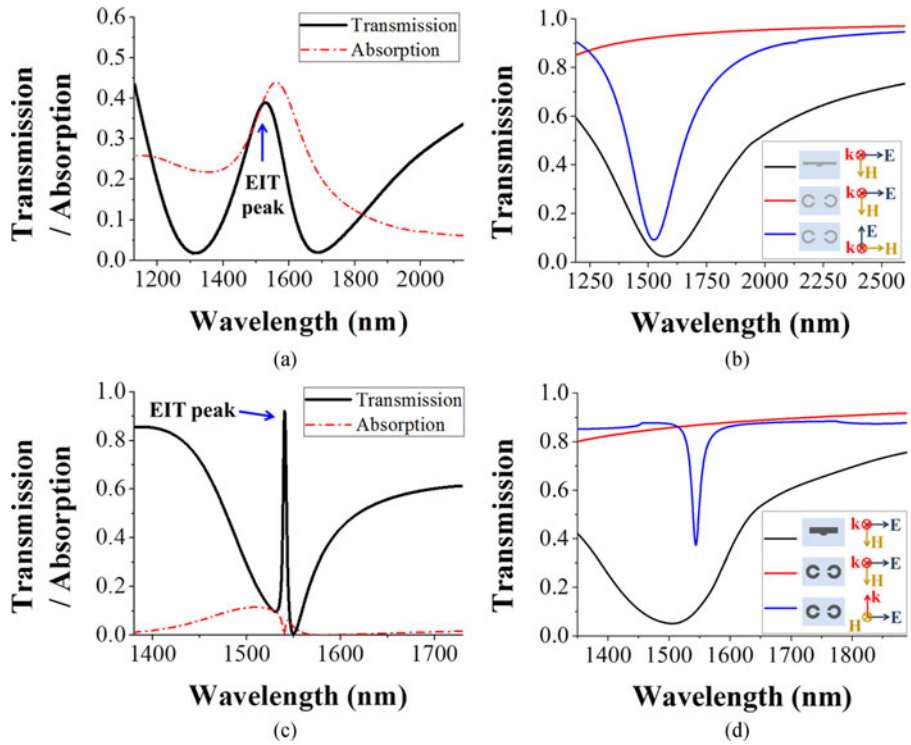

Fig. 2. Calculated transmission spectra for the (a) designed aluminum metamaterial comprised of both one bar resonator and two SRRs in the unit cell, (b) sole aluminum bar resonator and sole aluminum SRR pair pattern with two polarization directions of the incident electric field, (c) designed silicon metamaterial comprised of both one bar resonator and two SRRs in the unit cell, (d) sole silicon bar resonator and sole silicon SRR pair pattern with two incident directions. The absorption of the metamaterials is also shown in Fig. 2(a) and (b) with a red dotted line.

resonance can be directly excited by the same incident electromagnetic field in the SRR pair. There is no dip in the red curve of Fig. 2(d), because the magnetic polarization of the incident light is parallel to the plane where the SRR pair is located. On the other hand, we simulate the situation where the sole SRRs are excited by the input light at grazing incidence and with the magnetic field passing through the SRRs, as shown by the dip at approximately 1540 nm in the blue curve in Fig. 2(d). In this case, a magnetic dipole mode, instead of the LC resonance of the metallic metamaterial, is excited in the SRRs, in which the electric field and the displacement current whirl. In addition, if the E-field of the normal incident light is oriented along the *x*-axis and the SRR pair is placed in the same unit lattice with the bar, the SRRs can couple to the "bright mode" supported by the bar, given that the separation between the bar and SRR is small enough. The collective oscillations in the bar resonator excites the magnetic field rotating around itself. Furthermore, this magnetic field passes through the SRRs near the bar and excites the displacement current around the SRRs; this excitement leads to collective oscillation in the SRRs and suppression

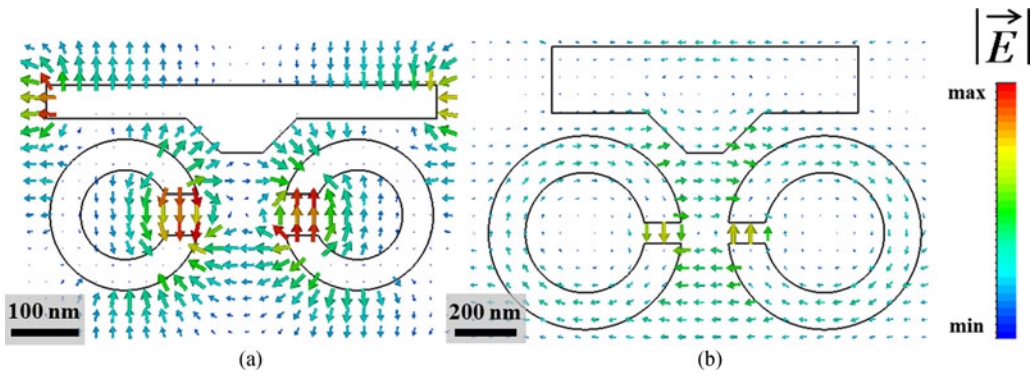

Fig. 3. The electric field distribution in the cross sections of the (a) aluminum metamaterial and (b) silicon metamaterial at half height (35 nm and 70 nm, respectively) and at the wavelength of EIT peak ($\lambda_1 = 1530$ nm, $\lambda_2 = 1540$ nm).

of radiative loss, forming the "dark mode" of the metamaterial. In conclusion, the interference between the "bright mode" and the "dark mode" leads to the EIT effect as shown in Fig. 2(c).

To further compare the EIT performance of the aluminum metamaterial and silicon metamaterial, we simulate the electric field distribution in the cross sections at half height (35 nm for the aluminum metamaterial and 70 nm for the silicon metamaterial) at the wavelength of EIT peak. The color of the arrow indicates the magnitude of the electric field intensity, $|\overrightarrow{E}|$, and the direction of the arrow indicates the direction of the electric field intensity. As shown in Fig. 3(a), most of the electric field is distributed in the split of the SRR pair, thus the LC resonance is excited in the SRRs and suppresses the LSP resonance in the bar resonator. In addition, the electric field is distributed on the surface of the metal structure and the surrounding medium, while there is no electric field inside the metal structure. As seen in Fig. 3(b), although the electric field in the split of the SRRs is the strongest because of the field enhancement based on the factor of $\varepsilon_d/\varepsilon_s$ (where ε_d is the permittivity of the resonator, and ε_s is the permittivity of the surrounding medium) [48], there is also some part of the electric field rotating along the SRRs. The electric field in the bar is the weakest because the radiative electric dipole is suppressed by the "dark mode". In other words, the dielectric material restricts part of the electric field to the interior of the structure.

The displacement current in dielectric metamaterials replaces the conduction current in the metallic counterparts; Mie-resonance in dielectric metamaterials replaces the LSP resonance. Consequently, energy loss, such as radiation loss and ohmic heat loss, is greatly reduced in dielectric metamaterials. Therefore, the Q-factors of both the "bright mode" and "dark mode" in the dielectric metamaterials are generally higher than the metallic counterparts in a similar waveband. High Q-factor resonances lead to high Q-factor EIT. Thus, the metallic EIT metamaterials with larger energy loss have a lower Q-factor than the dielectric EIT metamaterials with less energy loss.

On the other hand, the electric field is observed to be mostly distributed on the surface of the metal structure and the surrounding medium, while there is little electric field inside the metal structure, as shown in Fig. 3(a). In contrast, a significant electric field is observed to be inside the dielectric structure, as shown in Fig. 3(b). In addition, the electric field strength of the metal structure is also larger. These phenomena may result in higher sensitivity of the aluminum metamaterial to the ambient media.

In addition, we can see that part of the displacement current around the SRRs, between the isosceles trapezoid, changes direction (rotating along the SRRs) and points to the protrusion. This change in direction illustrates that much more of the electric field would be in contact with the ambient medium because of the coupling between the SRRs and protrusion, thus further enhancing the sensitivity towards the surroundings.

B. Comparison in the Application of Refractive Index Sensing

Refractive index (RI) sensing is one of the most interesting and common applications of the EIT metamaterials. The aluminum metamaterial and the silicon metamaterial are covered with different materials with RI ranging from 1.333 to 1.373. Fig. 4(a) and (c) show the simulated transmission spectra of the two metamaterials, respectively. Both EIT peaks of these two metamaterials shift along the long wavelength direction as RI increases. For the purpose of estimating the sensing property, the relationship between different RI and the wavelength shifts of two EIT peaks are shown in Fig. 4(b) and (d), respectively. After linear fitting, the sensitivities of these two peaks towards RI are determined to be 1642.97 nm/RIU and 433.05 nm/RIU, respectively. Both of the fitting degrees are 0.999, exhibiting good linear performance and the FOM of these two metamaterials are 11 and 116.7, respectively. The sensitivity of the aluminum metamaterial towards ambient RI is much larger than the silicon metamaterial counterpart in the same waveband; however the situation is the opposite when the Q-factor is considered, which verifies the estimation at the end of the previous section. In addition, the RI sensitivities of our designed metamaterials are higher in the near infrared waveband than their counterparts in most of the literatures, which may, to a certain extent, be due to coupling with the protruding isosceles trapezoids in the bar resonators.

It is also worth mentioning that in Fig. 4(a), although the sensitivity of the metallic EIT metamaterials is much larger, the line width of the EIT peak is usually wider due to the small

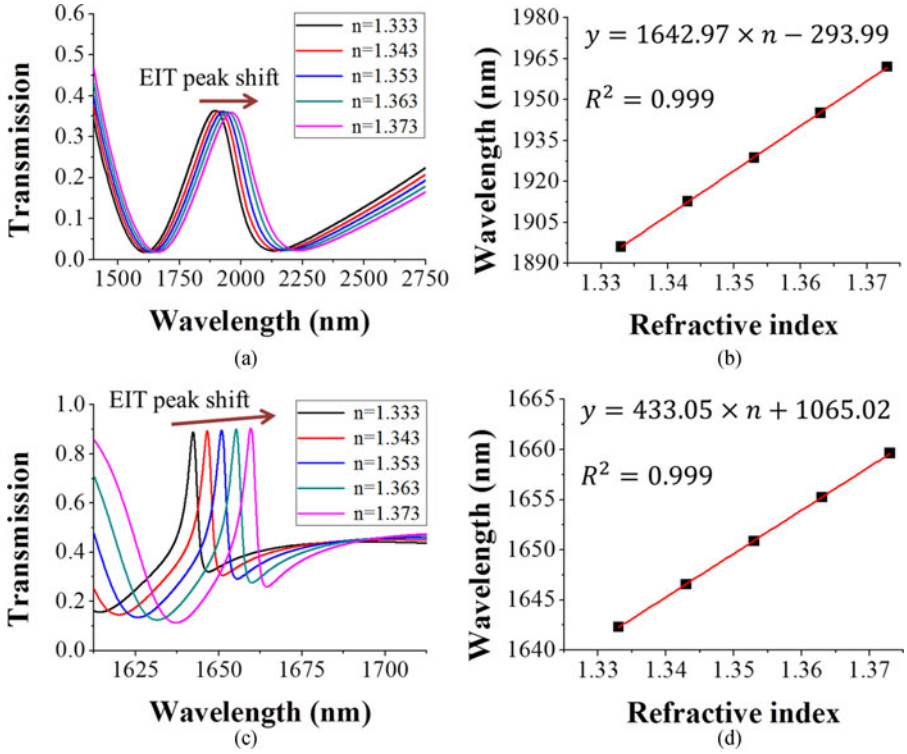

Fig. 4. (a) The transmission spectra of the aluminum metamaterial covered with different refractive index materials. (b) Linear fit of the relationship curves between the wavelength shift of the EIT peak and the external refractive index. (c) The transmission spectra of the silicon metamaterial covered with different refractive index materials. (d) Linear fit of the relationship curves between the wavelength shift of the EIT peak and the external refractive index.

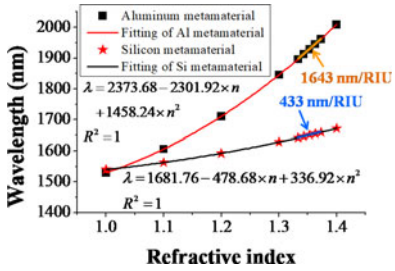

Fig. 5. Comparison of sensitivity between aluminum metamaterial and silicon metamaterial when ambient RI varies from 1 to 1.4.

Q-factor; this width is not beneficial in distinguishing small offsets when the wavelength interrogation method is used. One possible solution to this problem is to add a gain medium into the metal structure to reduce the energy loss, increase the Q value, and narrow the line width, such as [24]. The refractive index sensitivity of the dielectric metamaterials can also be increased by destroying the integrity of the structure while maintaining the continuity of the displacement current, such as [50], [65].

In Fig. 4(a), the spectral band of the investigating EIT peak in aluminium metamaterials does not correspond to the one shown in Fig. 4(c), which is designed in silicon material with similar structures. This is because of the tremendous difference in sensitivity. We also give a corresponding comparison of the RI sensitivity when RI varies from 1 to 1.4 in Fig. 5. The sensitivity of aluminium metamaterial is always higher than silicon metamaterial.

In our proposed metamaterial structure, there is an isosceles trapezoidal protrusion at the center of the bar resonator. We also further compared and analyzed the sensing performance of metamaterials with and without this isosceles trapezoidal protrusion, and the results are shown in Fig. 6(a) (aluminium metamaterial) and Fig. 6(b) (silicon metamaterial), respectively. And the electric field distributions in the cross sections of the metamaterials at half height of structures at the wavelength of EIT peak are inserted in Fig. 6. The color indicates the magnitude of the electric field intensity, $|\overrightarrow{E}|$. Both electric field distributions in Fig. 6(a) are in accordance with the same scale bar, and the inserts in Fig. 6(b) are also in accordance with the same scale bar. We can see clearly that both aluminium metamaterial and silicon metamaterial with isosceles trapezoidal protrusion have higher RI sensitivities than their own counterparts. The sensitivities can increase from 1181.3 nm/RIU (aluminium) and 320.8 nm/RIU (silicon) to 1642.97 nm/RIU (aluminium) and 433.05 nm/RIU (silicon), respectively. If we compare the electric field distribution of the metamaterials with and without protrusion, we can see clearly that the electric field intensity between protrusions (or the same place) and SRRs is enhanced after introducing the protrusions. This phenomenon is particularly evident in silicon metamaterial. It corresponds to the situation in Fig. 3 that some part of the displacement current (or surface current) around the SRRs changes original direction (rotating along the SRRs) and points to the protrusion and thus distributes in the ambient medium, which leads to the improvement of RI sensitivity. On the other hand, the RI sensitivity of aluminum metamaterial has much greater improvement than that of silicon metamaterials.

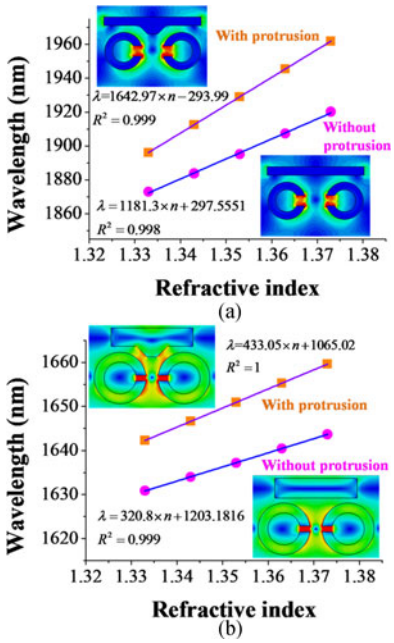

Fig. 6. (a) Comparison of sensitivity between aluminum metamaterial with and without protrusion at the middle of the bar. Inserts show the electric field distribution in the cross sections of the aluminium metamaterial at half height (35 nm) at the wavelength of EIT peak. (b) Comparison of sensitivity between silicon metamaterial with and without protrusion at the middle of the bar. Inserts show the electric field distribution in the cross sections of the silicon metamaterial at half height (70 nm) at the wavelength of EIT peak.

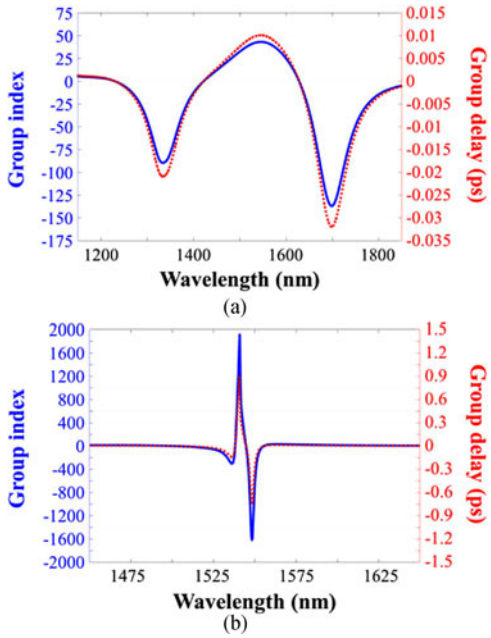

Fig. 7. Calculated group index (blue curve) and group delay (red dotted curve) of the (a) aluminum metamaterial and (b) silicon metamaterial.

This may because the introduction of the protrusions can increase the surface area of the aluminum metamaterials, and the SPR mode excited at the surface of plasmonic structure plays an important role in the sensing performance of the metallic structures. In a nutshell, both of these factors are helpful for improving the sensitivity of metamaterials and that is why the RI sensitivity of metamaterials we proposed are better than that of other metamaterials with similar structure (the bar and SRRs).

C. Comparison in the Application of Slow Light

It is well known that those EIT-like phenomena are always accompanied by the slow-light effect. We calculated the group index (blue curve) and group delay (red dotted curve) of the aluminum metamaterial and silicon metamaterial according to Eq. (2) and Eq. (3). To determine the effective phase, the effect of the substrate on the structure is removed by

$$\varphi = \varphi_T - \varphi_{\text{ref}} + kD \tag{6}$$

where φ_T is the transmission phase shift of metamaterial structure with substrate, φ_{ref} is the transmission phase shift of the same substrate without structure, k is the wave-number of free space, and D is the thickness of the metamaterial structure. The results are shown in Fig. 7(a) and (b); these results indicate that the silicon metamaterial has higher group index and optical delay than the aluminum metamaterial in the same waveband and comparable propagation distance. The maximum group delay of the aluminum metamaterial is 0.01 ps in the near infrared waveband. For the silicon metamaterial, the maximum group delay is as high as 0.89 ps in the near infrared waveband. We calculated the group index of the aluminum metamaterial and silicon metamaterial according to Eq. (3), where the maximum can reach 42.9 for the aluminum metamaterial and 1907.1 for the silicon metamaterial. The group delay and group index of our silicon metamaterial are both higher in the near infrared waveband than most of their counterparts in the literature. As can be derived from Eq. (2) and Eq. (3), the value of the group index and group delay is proportional to the derivative of the transmission phase shift relative to the frequency, i.e., $\frac{d\varphi(\omega)}{d\omega}$. It is also proportional to the Q-factor since the strong dispersion and phase mutation occurs at the EIT waveband. The larger the Q-factor is, the more rapidly the spectral curve changes, the more quickly the phase shifts, and the larger the derivative is. Thus, the EIT metamaterials with a larger Q-factor often have higher group index and optical delay than the metamaterials with a smaller Q-factor.

V. Conclusion

In summary, we investigated and summarized some of the literature on the EIT published to date. Then, aluminum and silicon metamaterials with similar glasses-shaped structures were designed for comparison of the metallic and all-dielectric metamaterials. Both consisted of a periodic lattice of one bar resonator and two SRRs. We analysed and compared the EIT performance in the near infrared waveband of these two metamaterials. The metallic EIT metamaterials with larger radiation loss and ohmic heat loss have smaller Q-factor than the dielectric counterparts with less energy loss. The Q-factors of the aluminum and silicon metamaterials are 10.06 and 412.6, respectively. However, the sensitivity to ambient refractive index of the aluminum metamaterial is 1642.97 nm/RIU, higher than that of the silicon metamaterial, 433.05 nm/RIU, which mainly caused by the electric field

strength and distribution variation. Furthermore, the sensitivities of our designed metamaterials towards RI are higher in the infrared waveband than their counterparts in most other literature which may, to a certain extent, be due to enhanced coupling with the isosceles trapezoids. For the application of slow light, the performance of the dielectric metamaterials with higher Q-factor is much better than that of the metallic metamaterials in the same waveband and comparable propagation distance. The group index of our designed aluminum metamaterial is 42.9 and the group delay is 0.01 ps at the EIT peak. For the silicon metamaterial, the group index is approximately 1907.1, and the group delay is as high as 0.89 ps within the transmission window in the near infrared waveband. The slow light effect of our silicon metamaterial is higher than most of its counterparts in the literature. The EIT metamaterials we designed have excellent performance, and to the best of our knowledge, it is the first time EIT metamaterials made of dielectric and metal with similar structure have been compared in detail; this paper may be meaningful for further research on the metamaterial analogues of EIT in the future.

REFERENCES

[1] K. Boller, A. Imamolu, and S. E. Harris, "Observation of electromagnetically induced transparency," *Phys. Rev. Lett.*, vol. 66, no. 20, pp. 2593–2596, May 1991.

[2] L. V. Hau, S. E. Harris, Z. Dutton, and C. H. Behroozi, "Light speed reduction to 17 m per second in an ultracold atomic gas," *Nature*, vol. 397, pp. 594–598, Feb. 1999.

[3] S. E. Harris and L. V. Hau, "Nonlinear optics at low light levels," *Phys. Rev. Lett.*, vol. 82, no. 23, pp. 4611–4614, Jun. 1999.

[4] C. L. Garrido Alzar, M. A. G. Martinez, and P. Nussenzveig, "Classical analog of electromagnetically induced transparency," *Amer. J. Phys.*, vol. 70, no. 1, pp. 37–41, Jan. 2002.

[5] D. D. Smith *et al.*, "Coupled-resonator-induced transparency," *Phys. Rev. A*, vol. 69, no. 6, pp. 063804–063808, Jun. 2004.

[6] L. Maleki, A. B. Matsko, A. A. Savchenkov, and V. S. Ilchenko, "Tunable delay line with interacting whispering-gallery-mode resonators," *Opt. Lett.*, vol. 29, no. 6, pp. 626–628, Mar. 2004.

[7] M. F. Yanik, W. Suh, Z. Wang, and S. H. Fan, "Stopping light in a waveguide with an all-optical analog of electromagnetically induced transparency," *Phys. Rev. Lett.*, vol. 93, no. 23, Dec. 2004, Art. no. 233903.

[8] A. Naweed, G. Farca, S. I. Shopova, and A. T. Rosenberger, "Induced transparency and absorption in coupled whispering-gallery microresonators," *Phys. Rev. A*, vol. 71, no. 4, Apr. 2005, Art. no. 043804.

[9] Q. Xu *et al.*, "Experimental realization of an on-chip all-optical analogue to electromagnetically induced transparency," *Phys. Rev. Lett.*, vol. 96, no. 12, Mar. 2006, Art. no. 123901.

[10] J. Xia *et al.*, "Electromagnetically induced transparency and absorption in a compact silicon ring-bus-ring-bus system," *Opt. Express*, vol. 25, no. 13, pp. 14368–14377, Jun. 2017.

[11] R. D. Kekatpure *et al.*, "Phase-coupled plasmon-induced transparency," *Phys. Rev. Lett.*, vol. 104, no. 24, Jun. 2010, Art. no. 243902.

[12] C. Zhen *et al.*, "Ultracompact chip-integrated electromagnetically induced transparency in a single plasmonic composite nanocavity," *Adv. Opt. Mater.*, vol. 2, no. 4, pp. 320–325, Feb. 2014.

[13] D. M. Yu *et al.*, "Plasmon-induced transparency in a surface plasmon polariton waveguide with a right-angled slot and rectangle cavity," *Plasmonics*, vol. 11, no. 4, pp. 1151–1155, Aug. 2016.

[14] Y. Wang *et al.*, "Plasmon-induced transparency effect in metal-insulator-metal waveguide coupled with multiple dark and bright nanocavities," *Opt. Eng.*, vol. 55, no. 2, p. 027108, Feb. 2016.

[15] W. Cai *et al.*, "Optical cloaking with metamaterials," *Nature Photon.*, vol. 1, no. 4, pp. 224–227, 2007.

[16] K. Aydin, I. Bulu, and E. Ozbay, "Subwavelength resolution with a negative-index metamaterial superlens," *Appl. Phys. Lett.*, vol. 90, no. 25, Jun. 2007, Art. no. 254102.

[17] C. Hu *et al.*, "Realizing near-perfect absorption at visible frequencies," *Opt. Express*, vol. 17, no. 13, pp. 11039–11044, 2009.

[18] Z. Li, H. Cheng, Z. Liu, S. Chen, and J. Tian, "Plasmonic airy beam generation by both phase and amplitude modulation with metasurfaces," *Adv. Opt. Mater.*, vol. 4, pp. 1230–1235, 2016.

[19] V. A. Fedotov, M. Rose, S. L. Prosvirnin, N. Papasimakis, and N. I. Zheludev, "Sharp trapped-mode resonances in planar metamaterials with a broken structural symmetry," *Phys. Rev. Lett.*, vol. 99, no. 14, Oct. 2007, Art. no. 147401.

[20] R. Singh *et al.*, "Observing metamaterial induced transparency in individual Fano resonators with broken symmetry," *Appl. Phys. Lett.*, vol. 99, no. 20, Nov. 2011, Art. no. 201107.

[21] N. Papasimakis, V. A. Fedotov, N. I. Zheludev, and S. L. Prosvirnin, "Metamaterial analog of electromagnetically induced transparency," *Phys. Rev. Lett.*, vol. 101, no. 25, Dec. 2008, Art. no. 253903.

[22] Z. Li *et al.*, "Manipulating the plasmon-induced transparency in terahertz metamaterials," *Opt. Express*, vol. 19, no. 9, pp. 8912–8919, Apr. 2011.

[23] J. S. Hwang *et al.*, "Bilayer metamaterial design for switchable electromagnetically-induced transparency-like response," *Current Appl. Phys.*, vol. 16, no. 4, pp. 469–474, 2016.

[24] Y. Sun, H. Chen, X. Li, and Z. Hong, "Electromagnetically induced transparency in planar metamaterials based on guided mode resonance," *Opt. Commun.*, vol. 392, pp. 142–146, 2017.

[25] D. Wu *et al.*, "Plasmonic metamaterial for electromagnetically induced transparency analogue and ultra-high figure of merit sensor," *Sci. Rep.*, vol. 7, Mar. 2017, Art. no. 45210.

[26] P. Tassin *et al.*, "Low-loss metamaterials based on classical electromagnetically induced transparency," *Phys. Rev. Lett.*, vol. 102, no. 5, Feb. 2009, Art. no. 053901.

[27] Z. G. Dong *et al.*, "Enhanced sensing performance by the plasmonic analog of electromagnetically induced transparency in active metamaterials," *Appl. Phys. Lett.*, vol. 97, Sep. 2010, Art. no. 114101.

[28] X. J. He, L. Wang, J. M. Wang, X. H. Tian, J. X. Jiang, and Z. X. Geng, "Electromagnetically induced transparency in planar complementary metamaterial for refractive index sensing applications," *J. Phys. D, Appl. Phys.*, vol. 46, no. 36, pp. 510–516, Sep. 2013.

[29] Z. Vafapour and H. Alaei, "Achieving a high Q-factor and tunable slow-light via classical electromagnetically induced transparency (Cl-EIT) in metamaterials," *Plasmonics*, vol. 12, no. 2, pp 479–488, Apr. 2017.

[30] P. Tassin *et al.*, "Planar designs for electromagnetically induced transparency in metamaterials," *Opt. Express*, vol. 17, no. 7, pp. 5595–5605, 2009.

[31] C. F. Ding *et al.*, "Reflection-type electromagnetically induced transparency analogue in terahertz metamaterials," *Chin. Phys. B*, vol. 23, no. 12, 2014, Art. no. 124203.

[32] H. M. Li, S. B. Liu, S. Y. Liu, and H. F. Zhang, "Electromagnetically induced transparency with large group index induced by simultaneously exciting the electric and the magnetic resonance," *Appl. Phys. Lett.*, vol. 105, Sep. 2014, Art. no. 133514.

[33] H. M. Li *et al.*, "Low-loss metamaterial electromagnetically induced transparency based on electric toroidal dipolar response," *Appl. Phys. Lett.*, vol. 106, no. 8, Feb. 2015, Art. no. 083511.

[34] X. Q. Lin *et al.*, "An EIT-based compact microwave sensor with double sensing functions," *IEEE Sens. J.*, vol. 16, no. 2, pp. 293–298, Jan. 2016.

[35] S. Han *et al.*, "Tunable electromagnetically induced transparency in coupled three-dimensional split-ring-resonator metamaterials," *Sci. Rep.*, vol. 6, 2016, Art. no. 20801.

[36] M. Manjappa *et al.*, "Magnetic annihilation of the dark mode in a strongly coupled bright–dark terahertz metamaterial," *Opt. Lett.*, vol. 42, no. 11, pp. 2106–2109, Feb. 2017.

[37] S. Zhang *et al.*, "Plasmon-induced transparency in metamaterials," *Phys. Rev. Lett.*, vol. 101, no. 4, Jul. 2008, Art. no. 047401.

[38] N. Liu *et al.*, "Plasmonic analogue of electromagnetically induced transparency at the Drude damping limit," *Nature Mater.*, vol. 8, no. 9, pp. 758–762, Jul. 2009.

[39] N. Liu *et al.*, "Planar metamaterial analogue of electromagnetically induced transparency for plasmonic sensing," *Nano Lett.*, vol. 10, no. 4, pp. 1103–1107, 2010.

[40] X. Liu *et al.*, "Electromagnetically induced transparency in terahertz plasmonic metamaterials via dual excitation pathways of the dark mode," *Appl. Phys. Lett.*, vol. 100, Mar. 2012, Art. no. 131101.

[41] X. Zhang *et al.*, "Polarization-independent plasmon-induced transparency in a fourfold symmetric terahertz metamaterial," *IEEE J. Sel. Topics Quantum Electron.*, vol. 19, no. 1, Jan./Feb. 2013, Art. no. 8400707.

[42] P. Pitchappa *et al.*, "Active control of electromagnetically induced transparency analog in terahertz MEMS metamaterial," *Adv. Opt. Mater.*, vol. 4, no. 4, pp. 541–547, Apr. 2016.
[43] J. Gu *et al.*, "Active control of electromagnetically induced transparency analogue in terahertz metamaterials," *Nature Commun.*, vol. 3, no. 4, Oct. 2012, Art. no. 1151.
[44] P. C. Wu *et al.*, "Magnetic plasmon induced transparency in three-dimensional metamolecules," *Nanophotonics*, vol. 1, no. 2, pp. 131–138, 2012.
[45] F. Shafiei *et al.*, "A subwavelength plasmonic metamolecule exhibiting magnetic-based optical Fano resonance," *Nature Nanotech.*, vol. 8, no. 3, pp. 95–99, Jan. 2013.
[46] Q. Zhao *et al.*, "Mie resonance-based dielectric metamaterials," *Mater. Today*, vol. 12, no. 12, pp. 60–69, 2009.
[47] A. Ahmadi and H. Mosallaei, "Physical configuration and performance modeling of all-dielectric metamaterials," *Phys. Rev. B, Condens. Matter*, vol. 77, no. 4, 2008, Art. no. 045104.
[48] F. L. Zhang *et al.*, "Magnetically coupled electromagnetically induced transparency analogy of dielectric metamaterial," *Appl. Phys. Lett.*, vol. 104, Mar. 2014, Art. no. 131907.
[49] J. Zhang *et al.*, "Electromagnetically induced transparency-like optical responses in all-dielectric metamaterials," *J. Opt.*, vol. 16, no. 12, Oct. 2014, Art. no. 125102.
[50] Y. Yang *et al.*, "All-dielectric metasurface analogue of electromagnetically induced transparency," *Nature Commun.*, vol. 5, Dec. 2014, Art. no. 5753.
[51] F. Zhang *et al.*, "Polarization and incidence insensitive dielectric electromagnetically induced transparency metamaterial," *Opt. Express.*, vol. 21, no. 17, pp. 19675–19680, Aug. 2013.
[52] L. Zhu and L. Dong, "Electromagnetically induced transparency with wide band in all-dielectric microstructure based on Mie resonances," *J. Opt.*, vol. 16, no. 16, Nov. 2014, Art. no. 125105.
[53] E. Petronijevic and C. Sibilia, "All-optical tuning of EIT-like dielectric metasurfaces by means of chalcogenide phase change materials," *Opt. Express*, vol. 24, no. 26, pp. 30411–30420, Dec. 2016.
[54] P. Ding *et al.*, "Electromagnetically induced transparency in all-dielectric metamaterial-waveguide system," *Appl. Opt.*, vol. 54, no. 12, pp. 3708–3714, Apr. 2015.
[55] S. G. Lee *et al.*, "Electromagnetically induced transparency based on guided-mode resonances," *Opt. Lett.*, vol. 40, no. 18, pp. 4241–4244, Sep. 2015.
[56] F. Zhang *et al.*, "Fano resonance of an asymmetric dielectric wire pair," *Appl. Phys. Lett.*, vol. 105, no. 17, Oct. 2014, Art. no. 172901.
[57] Z. Wei *et al.*, "Analogue electromagnetically induced transparency based on low-loss metamaterial and its application in nanosensor and slow-light device," *Plasmonics*, vol. 12, no. 3, pp. 641–647, Jul. 2017.
[58] D. R. Smith, D. C. Vier, T. H. Koschny, and C. M. Soukoulis, "Electromagnetic parameter retrieval from inhomogeneous metamaterials," *Phys. Rev. E.*, vol. 71, Mar. 2005, Art. no. 036617.
[59] D. R. Smith *et al.*, "Determination of effective permittivity and permeability of metamaterials from reflection and transmission coefficients," *Phys. Rev. B*, vol. 65, no. 19, 2002, Art. no. 195104.
[60] Z. Chen *et al.*, "Tunable electromagnetically induced transparency in plasmonic system and its application in nanosensor and spectral splitting," *IEEE Photon. J.*, vol. 7, no. 6, pp. 1–8, Dec. 2015.
[61] J. He and S. Yang, "Line shapes in a plasmonic waveguide system based on plasmon-induced transparency and its application in nanosensor," *Opt. Commun.*, vol. 381, pp. 163–168, Jul. 2016.
[62] J. Zhang *et al.*, "Strong field enhancement and light-matter interactions with all-dielectric metamaterials based on split bar resonators," *Opt. Express*, vol. 22, no. 25, pp. 30889–30898, 2014.
[63] P. C. Wu *et al.*, "Vertical split-ring resonator based nanoplasmonic sensor," *Appl. Phys. Lett.*, vol. 105, no. 3, pp. 033105–033108, Jul. 2014.
[64] P. C. Wu *et al.*, "Isotropic absorption and sensor of vertical split-ring resonator," *Adv. Opt. Mater.*, vol. 5, no. 2, Jan. 2017, Art. no. 1600581.
[65] J. Hu, T. Lang, and G. H. Shi, "Simultaneous measurement of refractive index and temperature based on all-dielectric metasurface," *Opt. Express*, vol. 25, no. 13, pp. 15241–15251, Jun. 2017.

Jie Hu was born in Zhejiang Province, China, in 1993. He received the Bachelor's degree in 2016 from China Jiliang University, Hangzhou, China, where he is currently working toward the Master's degree in the field of metamaterial optic biosensor.

Tingting Lang received the Bachelor's and Ph.D. degrees from the Department of Optical Engineering, Zhejiang University, Hangzhou, China, in 2004 and 2009, respectively.

She currently is an Associate Professor with the College of Optical and Electronic Technology, China Jiliang University, Hangzhou, China. Her current research interest is optical fiber sensing and metamaterials.

Zhi Hong received the Bachelor's and the M.S. degrees in electric engineering and the Ph.D. degree in optical engineering from Zhejiang University, Hangzhou, China, in 1984, 1987, and 2001, respectively.

He is currently a Professor, Doctoral Advisor, and the Director of the Centre for THz Research, China Jiliang University, Hangzhou, China. His current research interest is terahertz wave devices and sensor technology.

Changyu Shen was born in 1977 in Hunan, China. He received the M.S. degree in optics from Shanxi Normal University, Xi'an, China, in 2002 and the Ph.D. degree in optical engineering from Zhejiang University, Hangzhou, China, in 2009.

In 2013 and 2016, he was with the Advanced Photonic Components, Department of Electronics, Carleton University, Ottawa, ON, Canada, and the School of Physics, Trinity College Dublin, respectively, as a Visiting Scholar. He is currently a Professor with China Jiliang University, Hangzhou, China. His research interests include optics fiber sensors, tilted fiber Bragg Grating sensors, white light-emitting diodes, free space optical communication, and nonlinear optics.

Guohua Shi received the Bachelor's degree from the Department of Optoelectronic Information Engineering, Zhejiang University, Hangzhou, China, in 2003, and the Ph.D. degree in optical engineering from the Institute of Optics and Electronics, Chinese Academy of Sciences, Chengdu, China, under the supervision of Mr. Yudong Zhang.

He is currently a Professor and Doctoral Advisor, the Director of Medical Optics Technology Laboratory, Vice Director of the Key Medical Optics Laboratory of Jiangsu Province, Suzhou Institute of Biomedical Engineering and Technology, Chinese Academy of Sciences, Suzhou, China. His research focuses on the *in vivo* optical imaging and detecting method, as well as developing and industrializing the corresponding optical medical instruments.